Aalto University

OPEN ACCESS

This is an electronic reprint of the original article.
This reprint may differ from the original in pagination and typographic detail.

Scotti, Gianmario; Kanninen, Petri; Kallio, Tanja; Franssila, Sami

Integration of carbon felt gas diffusion layers in silicon micro fuel cells

Published in:
Journal of Micromechanics and Microengineering

DOI:
10.1088/0960-1317/22/9/094006

Published: 24/08/2012

Document Version
Peer-reviewed accepted author manuscript, also known as Final accepted manuscript or Post-print

Please cite the original version:
Scotti, G., Kanninen, P., Kallio, T., & Franssila, S. (2012). Integration of carbon felt gas diffusion layers in silicon micro fuel cells. *Journal of Micromechanics and Microengineering*, *22*(9), Article 094006. https://doi.org/10.1088/0960-1317/22/9/094006

This material is protected by copyright and other intellectual property rights, and duplication or sale of all or part of any of the repository collections is not permitted, except that material may be duplicated by you for your research use or educational purposes in electronic or print form. You must obtain permission for any other use. Electronic or print copies may not be offered, whether for sale or otherwise to anyone who is not an authorised user.

Integration of Carbon Felt Gas Diffusion Layers in Silicon Micro Fuel Cells

Gianmario Scotti[1,*], Petri Kanninen[2], Tanja Kallio[2] and Sami Franssila[1]
[1]Aalto University, Dept. of Materials Science and Engineering, PO Box 16200, FI-00076, Finland
[2]Aalto University, Dept. of Chemistry, P.O. Box 16100, FI-00076, Finland

*E-mail: gianmario.scotti@gmail.com

Abstract: We have integrated carbon felt, a traditional fuel cell gas diffusion layer, with silicon micro fuel cells. To this end we used two silicon microfabrication procedures using reactive ion etching: formation of black silicon and sinking of flowfield. The former decreases electrical contact resistance to the diffusion layer, the latter serves to contain the reactant gases. The micro fuel cells, where the flowfield was covered by black silicon nano-needles, showed better performance (127 mW cm^{-2}) compared to the same cells without black silicon (114 mW cm^{-2}). The black silicon fuel cells were also more stable during an overnight chronoamperometric measurement.

1. Introduction

Users of portable consumer electronic devices such as mobile phones, laptops, e-readers etc. benefit greatly from longer battery life. An avenue of research for a potential increase of the energy storage is by using micro fuel cells (MFC) [1]. These microfabricated devices should operate at low temperatures in order to be practical for portable applications, and should still have a high power density (per active area and per volume) so that a MFC system would be competitive to Li+ batteries in overall energy density. Using silicon for the microfabrication of MFCs has two advantages: readily available mature microfabrication techniques, and the integration of the device with the rest of the microelectronic circuitry [2-15].

The choice of gas diffusion layer (GDL) can significantly affect the performance of the fuel cell [16], but integration of a commercial GDL with a silicon chip is not a straightforward task. Kuriyama et al. [3] have grown multiwall carbon nanotubes (MWCNT) on a silicon wafer, and obtained a GDL of about 40 μm in thickness. To achieve this result, numerous deposition steps of various thin films, in addition to the MWCNT growth, were required. Xiao et al. [4] use lithographically defined 20 μm tall pillars etched in silicon, as a GDL, while Aravamudhan et al. [5] and Lee et al. [7] produced an array of holes in a silicon wafer, functioning as a macroporous diffusion layer. A similar kind of macroporous layer was implemented by Zhang, Advani et al [10] as an array of holes in a copper layer. Zhang, Lu et al [9] patterned the proton exchange membrane (PEM) with nanoimprint technology to create a thin microporous layer. Yeom et al [6] integrated a micro-porous GDL with their silicon chips by electroplating dendritic platinum black, up to 5 μm thick while the silicon substrate formed a macro-porous structure.

Unlike the researchers listed above, Kamitani et al. [13-15] integrated commercial macroporous and microporous layers into their silicon MFCs. The commercial micro-and-macroporous layers were placed on top of the silicon flowfield, but the electrical contact between flowfield and GDL was irrelevant, because in their set-up the flowfield was not a current collector; the authors used a gold mesh inserted between the flowfield and the GDL to collect the current. The fuel usage performance and the power density were both very high, for a methanol-fed and air-oxidant MFC.

In our previous work we have studied black silicon as a gas diffusion layer [2]. Black silicon is nanograss formed during plasma etching of silicon. Typically the silicon nanopillars are ca. 2 μm tall and a few hundred nanometers in diameter (Fig. 3c). While this approach had the advantage of very simple microfabrication, the thickness of the silicon nanograss layer cannot be extended much beyond 2 μm. Such a thin GDL may not be very beneficial for uniform gas flow and removal of water at the cathode, so we have introduced a thicker, commercial GDL (non-woven carbon felt) and integrated that into our silicon nanograss fuel cell. In our devices the flowfields also act as current collectors, and the electrical resistance between them and the GDL is a relevant factor. Stubenrauch et al. [17] have demonstrated that black silicon needles can achieve a good mechanical bonding with soft polymers. We will show that black silicon is also beneficial in forming a good electrical contact between silicon current collector and carbon felt GDL because of a Velcro-like attachment.

2. Experimental

2.1 Construction and microfabrication

The MFCs in this work are composed of two silicon flowfields which also perform the function of current collectors. For this purpose, the chips were fabricated from highly conductive (highly doped) silicon wafers, $\rho = 0.01\ \Omega$ cm. The membrane-electrode assembly (MEA) is a commercial product (Gore™ Primea®) with a Nafion®-based membrane and Pt loadings of 0.3 mg cm^{-2} and 0.1 mg cm^{-2} on the cathode and anode side respectively. Finally, a commercial carbon felt (E-Tek ELAT® GDL LT1200N) is integrated as GDL on the cathode and anode flowfields. Figure 1 (a) outlines the construction of one silicon chip which performs the functions of flowfield and current collector. Figure 1 (b) shows an exploded view of a MFC with all the components taken apart. The GDL is introduced inside the basin formed by sinking the flowfield by about 80 μm, with the macro-porous side turned towards the flowfield and the micro-porous side towards the MEA. The reactant gases enter the flowfield through one inlet hole and leave from the diagonally opposite one. All the dimensions pertaining to a single chip are summarized in table 1.

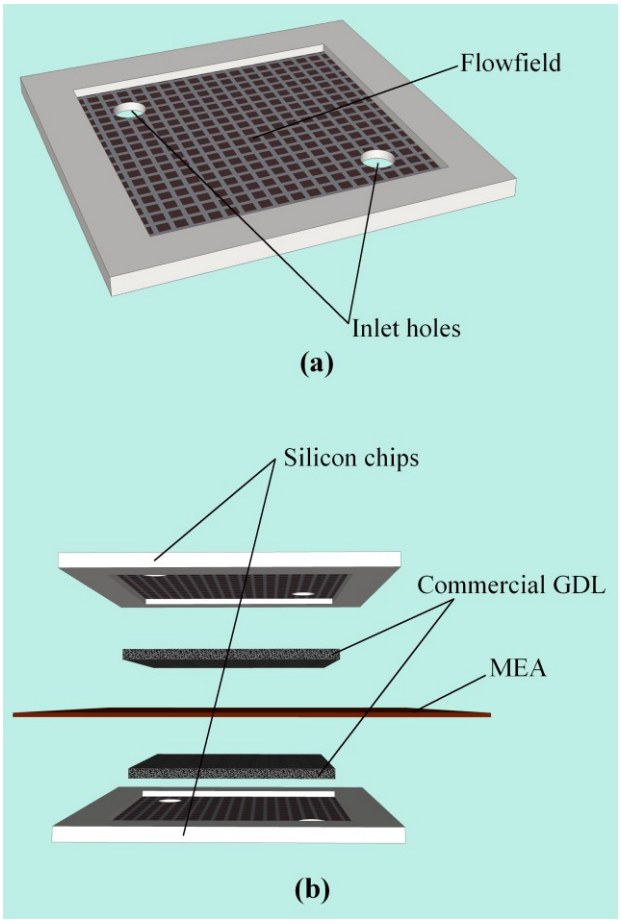

Figure 1. Construction of a flowfield/current collector silicon chip (a) and exploded view of a MFC (b).

Table 1. Characteristic dimensions of the MFC silicon chip.

Feature	Dimension
Flowfield area	10 x 10 mm^2
Chip thickness	400 µm
Flowfield channel depth	50 µm
Flowfield channel width	100 µm
Sinking of flowfield (basin depth)	80 µm
Inlet hole diameter	1 mm

Figure 2 illustrates the process flow for the fabrication of the silicon chips. A highly boron-doped, 400 µm thick silicon wafer is thermally oxidized with wet oxidation at 1050°C to form a 500 nm thick oxide layer. This layer is then patterned with photolithography (figure 2 (a)) and wet etching in a buffered HF

solution. This step opens up the flowfield area. Resist is spun on the top side and patterned to define the flowfield channels (b). The cured resist functions as mask for the deep reactive ion etching (DRIE) step (c). The resist is stripped and a subsequent DRIE step sinks the whole flowfield by about 80 μm (d); this being an anisotropic etch process, the bottom and the ridge of the channels will be sunk by the same amount. To create the inlet holes, through-wafer DRIE etching is performed from the back, where sputtered (200 nm thick) and lithographically patterned aluminum acts as hard mask (e). Finally, a RIE plasma etch in passivating conditions (high O_2 to SF_6 flow ratio) forms the black silicon nano-needles over the flowfield, and a 40 nm Au on 10 nm Ti-W adhesion layer is sputtered over the top of the wafer (f). The wafer is then diced in a diamond saw to separate the chips.

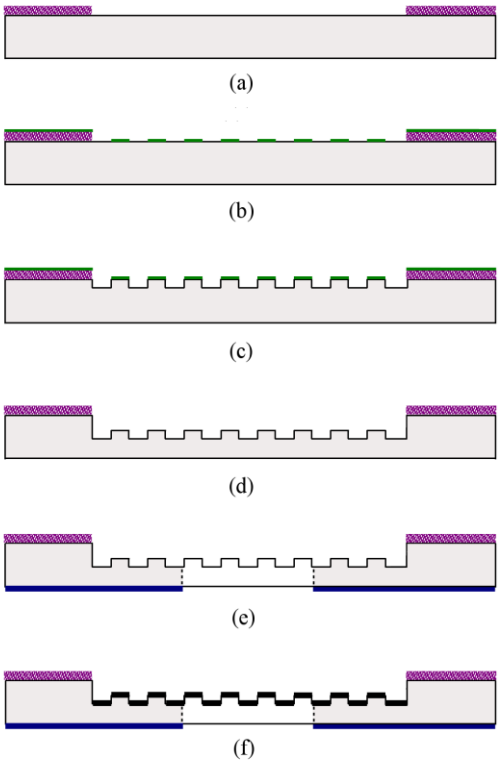

Figure 2. Process flow for the preparation of the silicon chip: pattern the SiO_2 to define the flowfield area (a), pattern the photoresist mask for the flowfield channels (b), RIE of flowfield channels (c), RIE to sink the flowfield (d), backside gas inlet etch through Al mask (e), and black silicon formation and metallization (f).

Two versions of the chips were prepared: ones with black silicon on the flowfield and the others without. Using both types, the effect black silicon has on the performance of a MFC can be assessed. The chips without black silicon were obtained by simply omitting the black silicon etch step (figure 2 (f)).

All RIE processing was done in an Oxford Instruments Plasmalab System 100®, a cryogenic inductively-coupled plasma (ICP) reactor. This device allows for the plasma and the plate RF powers to be separately adjusted. The process parameters are detailed in table 2. With the given parameters, the etch rate for the anisotropic etching of the channels, the sinking of the flowfield (basin formation) and through-wafer etch is 7 μm min^{-1}. The black silicon etch step lasts 8 minutes, which is sufficient to create black silicon needles of satisfactory morphology.

Table 2. RIE process parameters for silicon etching.

	Channel, basin and through-hole.	Black silicon.
Substrate temperature [ºC]	-110	-110
SF_6 flow [SCCM]	100	40
O_2 flow [SCCM]	15	18
ICP power [W]	2000	1000
RF power [W]	3	2

Figure 3 (a) is a photograph of the chips and an assembled MFC, next to a one euro coin, for size comparison. The top left chip is without black silicon, while the top middle chip has the black silicon treatment. Even though both chips are sputtered with gold, the characteristic yellow metallic color is not visible on the black silicon surface. The built-up MFC (right) reveals a portion of the MEA, cut to be slightly larger than the chips. Figure 3 (b) shows an optical micrograph of a used chip with black silicon. Strong illumination was utilized to take this picture. The top surface of the pillars is visible, even though black silicon reflects very little light [18], as is visible from the bottom of the flowfield and near the inlet hole. The reason for the visibility of the top of the pillars is that the chip was used in a MFC and the black silicon needles are damaged by the physical contact with the GDL, and do not absorb light quite as well as the black silicon at the bottom of the flowfield. A scanning electron microscopy (SEM) micrograph of a pillar with black silicon is presented in figure 3 (c).

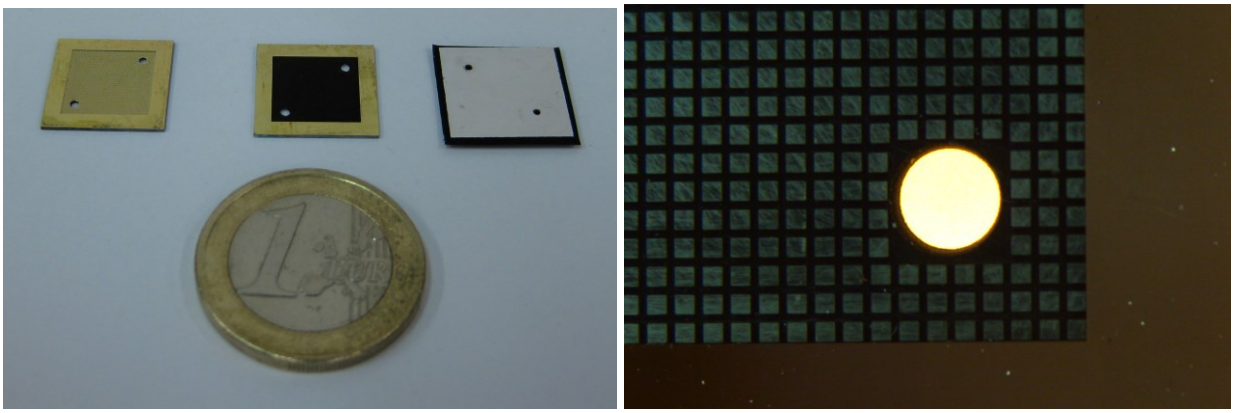

(a) (b)

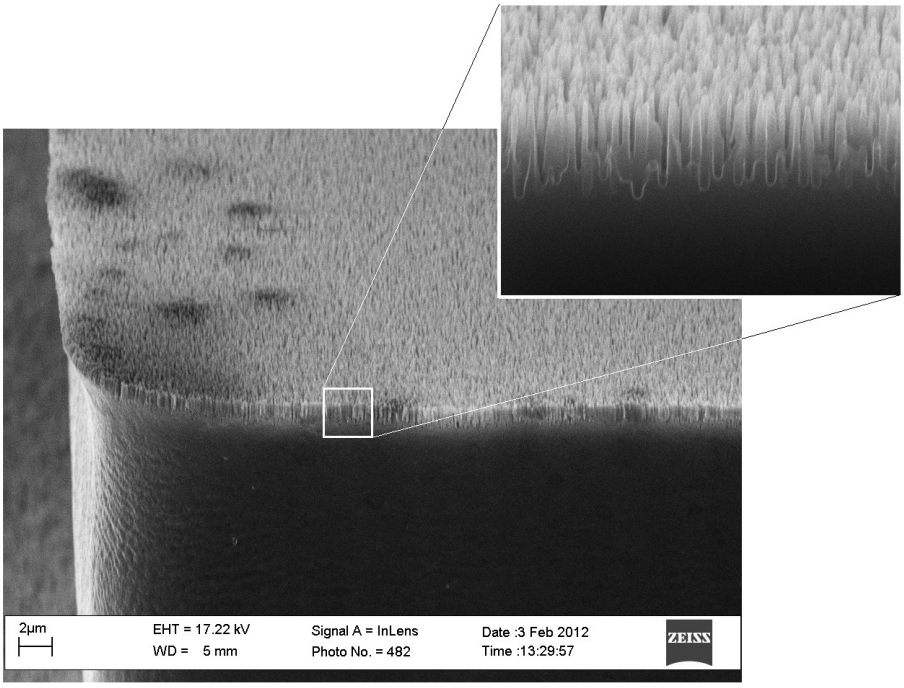

(c)

Figure 3. Photographs and micrographs of the micro fuel cells with and without black silicon. Photograph of the microfabricated chip without black silicon, with black silicon and an assembled MFC, next to a one euro coin (a). Optical microscope micrograph of a used chip with black silicon (b). SEM micrograph of black silicon on a square pillar. The inset is a higher magnification image of the black silicon at the edge (c).

The carbon felt is a non-woven compound structure where a microporous material such as carbon black, is screen-printed on a support fabric, the fibers of which are clearly visible on figure 4 (a) and (c). The side on which the printing is done is usually called microporous side, as the microporous material is predominant there. Conversely, the opposite side is called macroporous, and there is less carbon black

present. The microporous side, at the magnifications from figure 4 (b), looks essentially smooth, while the macroporous has a cavernous appearance, with still plenty of carbon black adhering to the support fibers (figure 4 (c)).

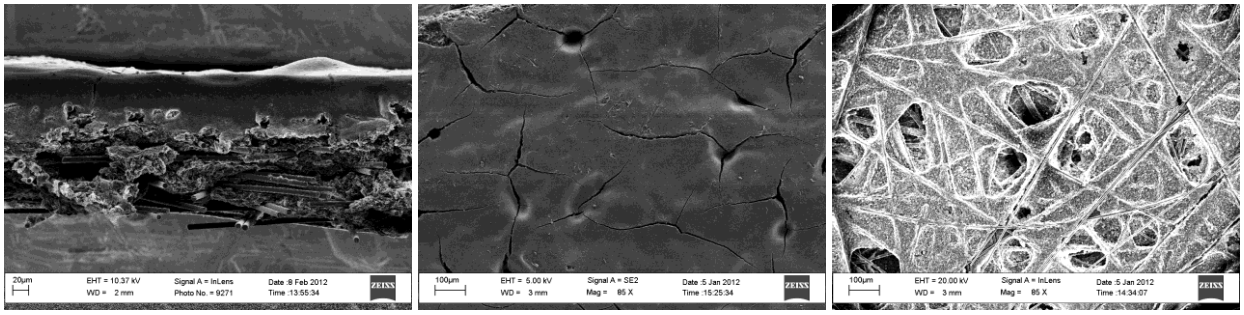

(a) (b) (c)

Figure 4. SEM micrographs of commercial carbon felt. Transversal section (a), top view from microporous side (b) and top view from macroporous side (c).

2.2 Characterization

The MFC were characterized by assembling and clamping them in a custom built aluminum jig (figure 5). The electric connections were made with the aluminum blocks that make up the jig, as they are in contact with the aluminum-metalized back of the chips. Gases were introduced into the cathode and anode flowfields through appropriate fittings threaded into the aluminum blocks. The flow was kept constant with the use of a Brooks Instrument® mass flow controller, at 50 mL min^{-1}. Current and voltage loading and data logging were done with a computer-controlled Metrohm Autolab PGSTAT100® potentiostat. Since the current generated by the fuel cells exceeded at times 350 mA, the potentiostat had to be connected to a current and voltage booster (Autolab BSTR10A®). The fuel is hydrogen, and the oxidant is either pure oxygen or air.

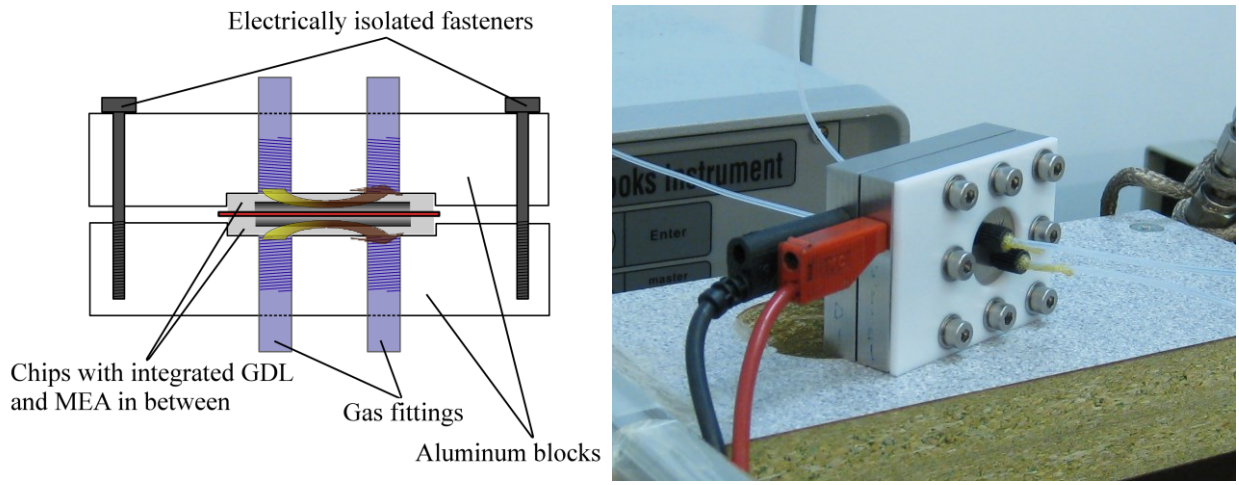

Figure 5. Diagram of the MFC inside the measurement jig (a) and photograph (b).

To measure the contact resistance between the flowfield (either with or without black silicon) and the carbon felt, a simple apparatus consisting of a pure copper cylinder (diameter 10 mm, mass 40 g) depicted in figure 6 was prepared. One side had a highly polished surface, which would press against the carbon felt. To the other side of the cylinder a thin copper wire was soldered, which in turn was connected to the potentiostat. The other electrode of the potentiostat is connected to one of the aluminum blocks from the previously described jig, in which one chip is placed with the flowfield facing upwards. The carbon felt is placed on the flowfield, either with the micro or the macroporous layer in contact with the flowfield. Before each measurement the polished side of the copper cylinder was cleaned with 0.1 M solution of HCl to remove any oxide layer, rinsed with de-ionized water and dried. In order to estimate the contact resistance over a range of currents, the Autolab potentiostat was used to sweep current from 0 to 30 mA over the assembly. The resulting current-voltage curve was linearized and the resistance obtained from the slope.

The chips used for this measurement did not have a basin (the flowfield was in the same plane as the surface of the wafer). The chips with and those without black silicon were fabricated from the same wafer, so all chips went through the exact same fabrication steps and conditions, except for the black silicon formation. This way the influence of fluctuations in process parameters and wafer characteristics was minimized.

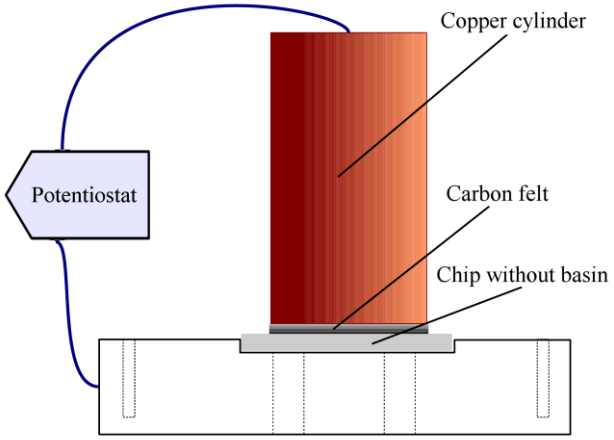

Figure 6. Resistance measurement apparatus. The bottom electrode is the aluminum block shown in figure 5.

Measurement of wetting properties of the black silicon and bare surfaces was conducted with contact angle measurements, using a KSV CAM 200® optical contact tensiometer. The measurements were performed on a wafer processed in the same way as the MFC chips, except that the patterning and the etch step for the flowfield were omitted. This was necessary as the smallest drop practically usable was still much larger than the flowfield pattern pitch, so measuring the contact angle on top of the flowfield would not have given useful results.

3. Results and discussion

3.1 Contact resistance measurements

Black silicon decreased the contact resistance between the carbon felt and the flowfield, because of their respective structures (Figures 3c and 4). The black silicon nanograss pierces into the microporous material, and increases contact area and electron conductivity between the current collector and the GDL. To verify this, the resistance was measured between the silicon chips (with and without black silicon) and the carbon felt, with the microporous side turned either towards the flowfield or the copper electrode, as described in the previous section (figure 6). The results are summarized in Table 3. The contribution of the bulk silicon resistance to the results reported is negligible, since it amounts to less than 0.4 mΩ.

Table 3. Contact resistance measurement results.

	Contact resistance [Ω].
A: Black silicon to macroporous layer	6.9 ± 1.4
B: Smooth surface to macroporous layer	9.6 ± 2.3
C: Black silicon to microporous layer	9.2 ± 1.8
D: Smooth surface to microporous layer	36.9 ± 7.4

In each instance where the flowfield with black silicon is in contact with the carbon felt (A and C), the resistance is smaller than in the case of the flowfield without the black silicon (B and D). The difference is much more drastic in the case of the microporous layer of the carbon felt turned towards the flowfield (C vs. D). This can be explained with the fact that on the microporous side there is a lot more carbon black material into which the black silicon can pierce. The smaller resistance of case A vs case C is due to the difference in contact resistance between the carbon cloth surfaces and the polished copper surface. In the case C, the cavernous macroporous side is turned towards the polished copper surface, and has hence a larger resistance than when the smoother microporous surface is turned towards the copper surface in case A. Therefore, the results in table 3 should be viewed as a combination of the contact resistance of the carbon felt's macro and microporous layers with the flowfield and the polished copper surface.

It can be concluded that black silicon clearly reduces resistance between the flowfield of the silicon chip and the carbon felt, regardless whether the micro or the macroporous side is turned towards the flowfield. SEM images after contact resistance measurements showed no damage to the black silicon nano-needles, regardless of which side of the carbon felt was pressed against them.

3.2 MFC performance

The measurements were done on several MFCs, and typical scans are reported. Polarization curves (figure 7) were done by sweeping the voltage from open-circuit (OCV) to 0.2 V and measuring the produced current. This was done before and after a chronoamperometry (CA) experiment, where potential was held constant at 0.4 V for approximately 20 hours, and the current was measured (figure 8). In these measurements, oxygen was the oxidant. Both before and after the long-term load of the MFCs, the cells with black silicon produced a higher current and power density than the ones with smooth surface. In terms of maximum power densities, the black silicon cells produced 10% more power before the CA (127 vs. 114 mW cm^{-2}) and 50% more after the CA (97 vs. 63 mW cm^{-2}). The same trend can be observed from the CA: MFCs with black silicon exhibit a consistent improvement in performance compared to the MFCs with smooth surface, during the whole period of 20 hours.

Water management is an important part of a functioning fuel cell. The cathodic reaction produces water and at high current densities it can block the catalyst sites [19]. One reason for improved performance of the MFCs with black silicon in addition of better electrical contact could be that black silicon helps the removal of water from the fuel cell. To further study the effect of water in the cells, cyclic voltammetry (CV) was performed before and after CA.

In a CV, the voltage was swept from OCV to 0.05 V (forward sweep) and back to OCV (backward sweep). Generally, it can be seen that higher current densities are observed with the forward sweep going to low voltages. The effect is especially pronounced with black silicon as it is tested just after assembly. The difference in CVs between the black silicon and smooth cells is likely to be caused by effects on the flowfield as the two types of fuel cells are identical except for the flowfield surface. Therefore, the causes are most likely limited to mass transfer of the reactants and products between the flowfield and the carbon felt as no chemical reactions happen in the flowfield. Considering that the differences between the CVs of the black silicon cells and the smooth cells are pronounced at high current densities of forward and backward sweeps, it is likely that the poorer performance of the black silicon chip there is caused by the water formed at the high current densities. After the CA measurement, both cell types exhibit smaller hysteresis. As the maximum currents of both cell types have decreased, the first reason to this is the reduced amount of water produced at low potentials. It is also possible that liquid water pathways are formed in the carbon felt as the cell gets wetter during the CA measurement and this helps the water flow out of the cell easier. It is however clear that the black silicon fuel cell offers better stability and performance in the long run. This could be due to the more intimate electrical contact between the black silicon chip and the carbon felt remaining better as the cell is getting more humid. More detailed experiments with hydrogen and oxygen of different relative humidity at input would be required to study this effect more deeply.

Post-mortem SEM investigation of the black silicon chips used in the MFC characterization experiments show damage to the nano-needles, unlike the chips used for contact resistance measurements. Regions of large damage (figure 10 a), and those without any damage (figure 10 b) are randomly distributed in close proximity, on each surface in contact with the carbon felt. The broken black silicon debris could affect mass transfer during the first CV sweeps. Part of this debris would gradually seep out during the CA measurement possibly accounting for part of the effect seen on CV curves.

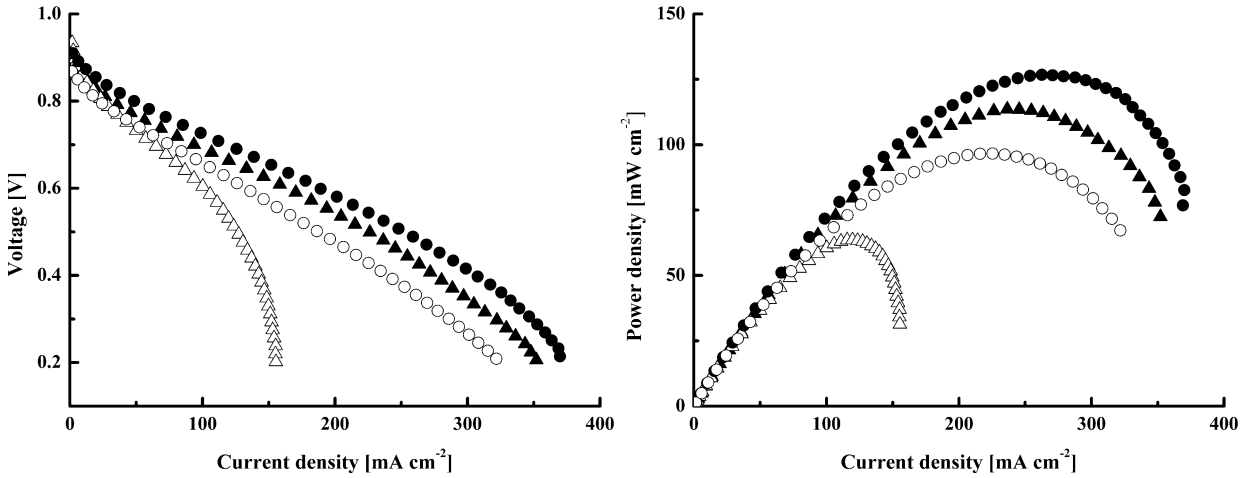

(a) (b)

Figure 7. Current density (a) and power density (b) polarization curves of the MFCs with oxygen as oxidant. Circles indicate polarization curves for MFCs with black silicon, triangles for MFCs with smooth surfaces. Black symbols are for curves measured before the chronoamperometric measurement, white symbols after the chronoamperometric measurement.

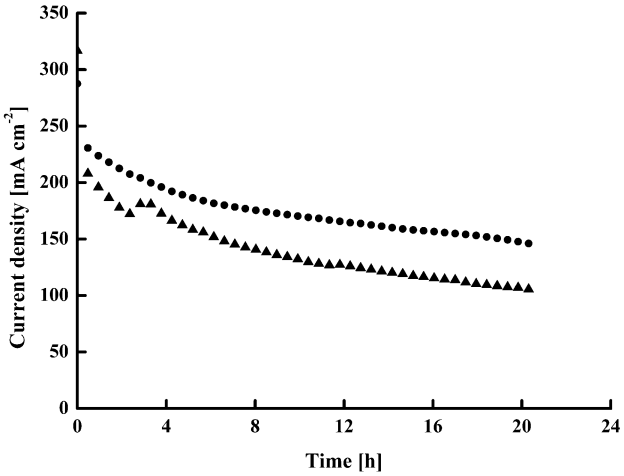

Figure 8. Chronoamperometric measurements. Circles indicate graphs for MFCs with black silicon, triangles for MFCs without black silicon.

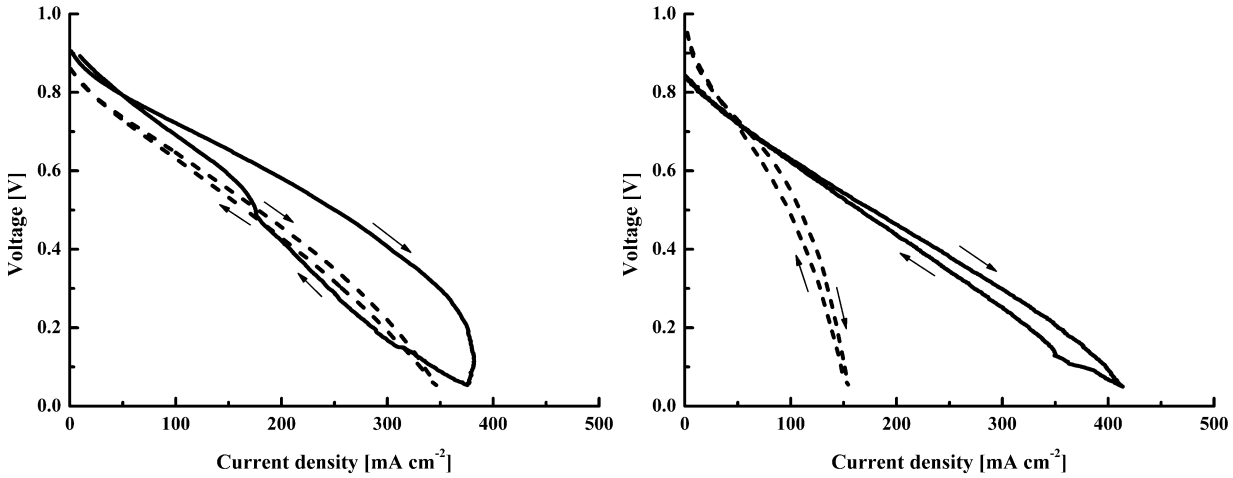

(a) (b)

Figure 9. Cyclic voltammetry (CV) measured on MFCs with oxygen as oxidant. With black silicon (a) and with smooth surfaces (b). CVs performed before the chronoamperometric measurement are drawn with full lines, while those performed after it are drawn with dashed lines.

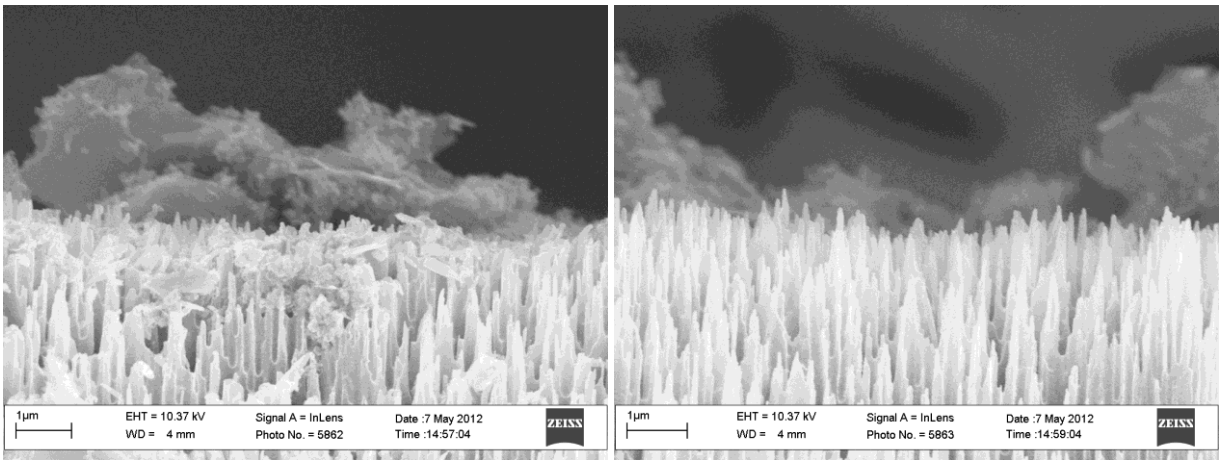

(a) (b)

Figure 10. SEM micrographs of black silicon surface of used MFC chips. Local damage is seen at random locations (a) while neighboring areas are unaffected (b).The two image sites are 10 µm apart. Fragments of the carbon felt are visible in the background on both micrographs.

After the chronoamperometric measurement and the final polarization and CV sweeps, the oxygen source was replaced with an air source, and the polarization curves on figure 10 were obtained. The MFCs with black silicon produce a higher current density than the ones with smooth surface – more than twice as high at 0.2 V – which translates into a higher power density: 16 mW cm^{-2} vs. 10 mW cm^{-2} for MFCs with

black silicon vs. MFCs with smooth surfaces, respectively.

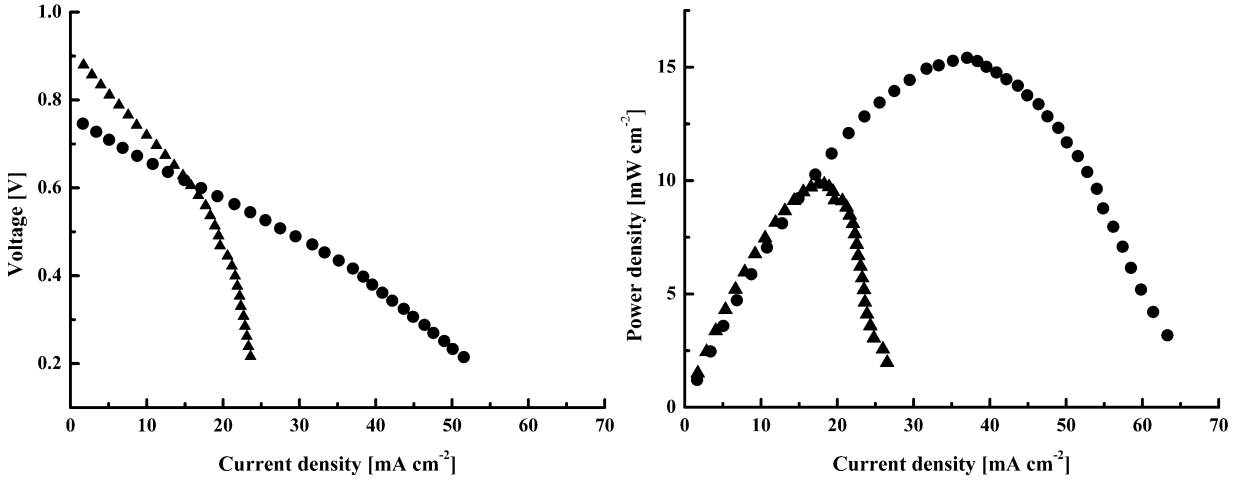

(a) (b)

Figure 11. Current density (a) and power density (b) polarization curves obtained with air as oxidant. Circles indicate graphs for MFCs with black silicon, triangles for MFCs without black silicon.

To gain a better insight into the possible reasons behind the effect of black silicon on MFC water management, contact angle measurements were conducted.

3.3 Contact angle measurements

Black silicon can have interesting wetting properties; it can be made super-hydrophobic or super-hydrophilic [20], depending on surface coating. To ascertain the wetting properties of the black silicon and the smooth surfaces in our MFCs (both with sputtered gold), contact angle measurements on a wafer without flowfield channels and through-holes were made. The samples were subjected to conditions mimicking those of the MFC chips. Before dicing, the wafer was covered with photoresist to protect the fine structures of the black silicon surface from mechanical damage. This resist was stripped with acetone, after dicing. For this reason, some of the samples were dipped in acetone, while others were covered with photoresist which was then later stripped with acetone. The 15 minute deionized (DI-) water dip (and subsequent drying) was necessary to measure the effects of water condensation on the microchannel walls, during MFC operation. The results of all these measurements are summarized in table 4.

One hour after 40 nm of gold (with 10 nm Ti-W adhesion layer) was sputtered on the sample, both the smooth and the black silicon surfaces showed extremely high wettability with water: the contact angles measured were below 5º for both kinds of surfaces. This was not entirely surprising, as the contact angle

of water on metals (unlike with polymers and other dielectrics) is highly dependent on the history of the surface [21], and freshly polished gold surface is known to be super-hydrophilic. Indeed, 48 hours later while the wafer was resting in a closed sample holder outside the cleanroom, the surfaces exhibited contact angles of about 120º and 90º degrees for the black silicon and the smooth surfaces respectively. With a contact angle of about 90° on the smooth surface, the contact angle of 120º on black silicon is actually an advancing contact angle, caused by pinning on the black silicon nanograss [20] and is not necessarily a reliable indication of the actual wettability of the surface. However, when the contact angle on the smooth surface differs more considerably from 90°, the black silicon measurements are more significant. It can be concluded that, after each of the treatments (DI-water, acetone or acetone stripping of photoresist), the smooth surface becomes slightly hydrophilic (66°-77°), while the black silicon surface becomes more hydrophilic than the smooth surface (25°-53°).

Table 4. Contact angle measurement results.

	Black silicon [°].	Smooth surface [°].
Freshly sputtered with Au/Ti-W	< 5	< 5
After 48 h air exposure	120	89
After DI water dip of 15 min.	41	77
After acetone dip of 15 min.	25	66
After photoresist stripping with acetone	53	67
Water spraying	76	69

In summary, it is correct to assume that, during usage, both the smooth as well as the black silicon surfaces in the MFC will become hydrophilic to some extent. It is also clear that, in any case, the black silicon surface will become more hydrophilic than the smooth surface, but it will not become super-hydrophilic. As the change of the contact angle is generally larger for the black silicon case, it can also explain why the change in the hysteresis before and after the CA measurement is larger for black silicon cells than it is for the smooth cells in addition to the reduced current densities (less water production), improved flow of water through the carbon felt and black silicon debris removal.

It is also noteworthy that the black silicon responds to exposure to DI water and acetone more slowly than smooth surface. There is a large difference in the contact angles of black silicon that was only sprayed with water or acetone compared to black silicon that was dipped into them. On the other hand, smooth silicon surface seems to respond similarly to both the spraying and the dipping of DI water and acetone. In other words, the contact angle of black silicon surface is dependent on the time of the water and acetone exposure, whereas the contact angle of the smooth silicon surface reaches fixed value almost

immediately (the spraying lasted only for a few seconds). It is thus possible that the flowfield with the smooth surface has reached equilibrium in regards to water before the CA measurement. For the black silicon this process takes a longer time and this delay results in stronger hysteresis in the beginning of the measurements.

There have been some studies of water transport in hydrophilic and hydrophobic macroscopic flow channels [22-25], but no consensus about their effects has been found. On hydrophilic walls, water forms thin films that do not substantially obstruct the gas flow. The gas flow will then push the water film towards the exit of the cell. On the other hand, on hydrophobic walls water forms droplets which are propelled out of the cell quickly because of increasing pressure behind them. From experimental [25] and modeling results [22], flow field contact angles around 90° indicate most water retained in the channels and thus poor performance. However, fuel cell measurements with two flow field surfaces closely matching the contact angles of smooth and black silicon surfaces (40° and 95°) [23] did not indicate large differences during single polarization curves. It seems that in the microscale the surface properties play a larger role and therefore their effect to the overall performance of the fuel cell is more significant as indicated by our results.

4. Conclusion

The resistance measurements, which were performed in a controlled and repeatable environment together with the various fuel cell characterizations indicate that the simple step of forming black silicon over the flowfield surface does decrease flowfield-to-GDL resistance. This step is easy to integrate in the process of microfabrication of the MFC chip, as it is done in the same reactor where the flowfield is etched, and it lasts only 8 minutes. It uses the same reactant gases as the anisotropic etch process, and therefore it is easily available to researchers working with silicon-based MFCs.

Acknowledgements

We would like to express our gratitude to our colleagues Ville Jokinen for useful discussions on the topic of surface tension and wettability of black silicon, and Maija Mäkinen for helping with micro fuel cell characterization. We would also like to acknowledge MIDE, Aalto University, Finland, for the funding of the project.

References

[1] Kundu A, Jang J H, Gil J H, Jung C R, Lee H R, Kim S-H, Ku B and Oh Y S 2007 *J. Power*

Sources **170** 67-78
[2] Scotti G, Kanninen P, Mäkinen M, Kallio T and Franssila S 2010 Silicon nanograss as micro fuel cell gas diffusion layer *Micro Nano Lett.* **5** 382-385
[3] Kuriyama N, Kubota T, Okamura D, Suzuki T and Sasahara J 2008 Design and fabrication of MEMS-based monolithic fuel cells *Sens. Actuators, A* **145-146** 354-362
[4] Xiao Z, Yan G, Feng C, Chan P C H and Hsing I M 2006 A silicon-based fuel cell micro power system using a microfabrication technique *J. Micromech. Microeng.* **16** 2014-2020
[5] Aravamudhan S, Rahman A R A and Bhansali S 2005 Porous silicon based orientation independent, self-priming micro direct ethanol fuel cell *Sens. Actuators, A* **123-124** 497-504
[6] Yeom J, Mozsgai G Z, Flachsbart B R, Choban E R, Asthana A, Shannon M A and Kenis P J A 2005 Microfabrication and characterization of a silicon- based millimeter scale PEM fuel cell operating with hydrogen, methanol, or formic acid, *Sens. Actuators, B* **107** 882-891
[7] Lee C Y, Lee S J, Hu Y C, Shih W P, Fan W Y and Chuang C W 2009 Integration of silicon micro-hole arrays as a gas diffusion layer in a micro-fuel cell, *Int. J. Hydrogen Energy* **34** 2009 6457-6464
[8] Wozniak K, Johansson D, Bring M, Sanz-Velasco A and Enoksson P 2004 A micro direct methanol fuel cell demonstrator *J. Micromech. Microeng.* **14** S59-63
[9] Zhang Y, Lu J, Shimano S, Zhou H and Maeda R 2007 Development of MEMS based direct methanol fuel cell with high power density using nanoimprint technology *Electrochem. Commun.* **9** 1365-8
[10] Zhang F-Y, Advani S G and Prasad A K 2008 Performance of a metallic gas diffusion layer for PEM fuel cells *J. Power Sources* **176** 293-298
[11] Torres N, Santander J, Esquivel J P, Sabaté N, Figueras E, Ivanov P, Fonseca L, Gràcia I and Cané C 2008 Performance optimization of a passive silicon-based micro-direct methanol fuel cell *Sens. Actuators B* **132** 540-544
[12] Esquivel J P, Sabaté N, Santander J, Torres N and Cané C 2008 Fabrication and characterization of a passive silicon-based direct methanol fuel cell *Microsyst. Technol.* **14** 535-541
[13] Kamitani A, Morishita S, Kotaki H and Arscott S 2008 Miniaturized microDMFC using silicon microsystems techniques: performances at low fuel flow rates *J. Micromech. Microeng.* **18** 125019
[14] Kamitani A, Morishita S, Kotaki H and Arscott S 2009 Improved fuel use efficiency in microchannel direct methanol fuel cells using a hydrophilic macroporous layer *J. Power Sources* **187** 148-155
[15] Kamitani A, Morishita S, Kotaki H and Arscott S 2011 Microfabricated microfluidic fuel cells *Sens. Actuators B* **154** 174-180
[16] Cindrella L, Kannan A M, Lin J F, Saminathan K, Ho Y, Lin C W and Wertz J 2009 *J. Power Sources* **194** 146-160
[17] Stubenrauch M, Fischer M, Kremin C, Hoffman M and Müller J 2007 Bonding of silicon with filled and unfilled polymers based on black silicon *Micro Nano Lett.* **2** 6-8
[18] Sainiemi L, Jokinen V, Shah A, Shpak M, Aura S, Suvanto P and Franssila S 2010 Non-Reflecting Silicon and Polymer Surfaces by Plasma Etching and Replication *Adv. Mater.* **23** 122-126
[19] Pekula N, Heller K, Chuang P A, Turhan A, Mench M M, Brenizer J S and Ünlü K 2005 Study of water distribution and transport in a polymer electrolyte fuel cell using neutron imaging *Nucl Instrum. Methods Phys. Res. Sect. A* **542** 134–141
[20] Jokinen V, Sainiemi L and Franssila S 2008 Complex Droplets on Chemically Modified Silicon Nanograss *Adv. Mater.* **20** 3453-3456
[21] Bewig K W and Zisman W A 1965 The Wetting of Gold and Platinum by Water *J. Phys. Chem.* **69** 4239-4242
[22] Quan P and Lai M-C 2006 Numerical study of water management in the air flow channel of a PEM fuel cell cathode *J. Power Sources* **164** 222-237
[23] Owejan J P, Trabold T A, Jacobson D L, Arif M and Kandlikar S G 2007 Effects of flow field and diffusion layer properties on water accumulation in a PEM fuel cell *Int. J. Hydrogen Energy* **32** 4489-4502

[24] Yang X G, Zhang F Y, Lubawy A L and Wang C Y 2004 Visualization of Liquid Water Transport in a PEFC *Electrochem. Solid-State Lett.* **7** A408-A411
[25] Tang H-Y, Santamaria A, Park J W, Lee C and Hwang W 2011 Quantification of water in hydrophobic and hydrophilic flow channels subjected to gas purging via neutron imaging *J Power Sources* **196** 9373-9381